ELSEVIER

Contents lists available at ScienceDirect

Acta Biomaterialia

journal homepage: www.elsevier.com/locate/actbio



Full length article

pH-responsive silk fibroin-based CuO/Ag micro/nano coating endows polyetheretherketone with synergistic antibacterial ability, osteogenesis, and angiogenesis



Jianglong Yan^a, Dandan Xia^b, Wenhao Zhou^f, Yangyang Li^a, Pan Xiong^{a,d}, Qiyao Li^c, Pei Wang^a, Ming Li^e, Yufeng Zheng^{b,*}, Yan Cheng^{a,*}

- ^a Academy for Advanced Interdisciplinary Studies, Peking University, Beijing 100871, China
- ^b Department of Materials Science and Engineering, College of Engineering, Peking University, Beijing 100871, China
- ^cDepartment of Biomedical Engineering, Materials Research Institute, Huck Institutes of the Life Sciences, The Pennsylvania State University, University Park, PA 16802, USA
- ^d The Science and Technology Bureau of Chengdu, Chengdu Administration of Foreign Experts Affairs, Chengdu 610042, China
- ^e China-America Institute of Neuroscience, Xuanwu Hospital, Capital Medical University, Beijing 100053, China
- ^fShaanxi Key Laboratory of biomedical metal materials, Northwest Institute for Non-ferrous Metal Research, Xi'an 710016, China

ARTICLE INFO

Article history: Received 19 May 2020 Revised 29 July 2020 Accepted 31 July 2020 Available online 7 August 2020

Keywords: Copper/silver Polyetheretherketone Angiogenesis pH-responsive antibacterial Osseointegration

ABSTRACT

Polyetheretherketone has been widely used for bone defect repair, whereas failures may happen due to implant loosening and infection. Thus, PEEK implant with multi-function (osteogenesis, angiogenesis, and bacteria-killing) is essential to solve this problem. Herein, copper oxide microspheres (μ CuO) decorated with silver nanoparticles (nAg) were constructed on porous PEEK surface via silk fibroin. In vitro studies highlighted the pH controlled release ability of this coating. It liberated a high dose of Cu²⁺ and Ag⁺ at low pH environment (pH 5.0), leading to 99.99% killing of planktonic bacteria and complete eradication of sessile bacteria, avoiding biofilm formation. Under physiological environment (pH 7.4), a lower amount of leaked metal ions induced promoted ALP production, collagen secretion, and calcium deposition, as well as NO production, which indicated potentiated osteogenesis and angiogenesis. *In vivo* results displayed the highest new bone volume around, and the appearance of new bone inside porous structure of, PEEK implant with this coating in rabbit tibia, signified the abilities of this coating to promote bone regeneration and osseointegration. Our study established solid support for implants with this coating to be a successful bone defect repair solution.

Statement of Significance

In this study, CuO/Ag micro/nano particles were incorporated into the porous surface of PEEK through polydopamine and silk fibroin layers. The design of this coating conferred pH-controlled release behavior to Cu²⁺ and Ag⁺. High dose of metal ions were released at pH 5.0, which presented synergistic antibacterial ability and killed 99.99% of planktonic bacteria. Low concentration of metal ions were controlled by this coating at physiological environment, which potentiated osteodifferentiation of Ad-MSC in vitro and led to complete integration of implant with bone tissue *in vivo*.

© 2020 Acta Materialia Inc. Published by Elsevier Ltd. All rights reserved.

1. Introduction

The requirement for bone defects treatment remains a big evergrowing challenge in the orthopedic area worldwide, and there

E-mail addresses: yfzheng@pku.edu.cn (Y. Zheng), chengyan@pku.edu.cn (Y. Zheng).

are about 1 million cases per year that require bone grafting due to congenital diseases, trauma and tumor resection. The autograft had been considered the standard of bone graft replacement, and allograft is alternative to autograft. However, natural bone grafts and implants have several limitations such as disease transfer, limited availability and reproducibility, donor scarcity, and host immune rejection [1]. These worries led the researchers incline towards using synthetic bone grafting. Polyetheretherketone (PEEK),

^{*} Corresponding authors.

a semi-crystalline polymer, is a promising alternative materials [2]. Compared with titanium alloys and other alloys, PEEK shows robust chemical resistance. Therefore there is no concerns about metal ions released by degradation and corrosion, which may lead to systemic allergic or aseptic loosening [3]. Additionally, PEEK possesses relatively lower elastic modulus which is similar to cortical bone, minimizing the stress shielding effect [4]. However, PEEK possesses inherent bioinertness, leading to insufficient osseointegration and implant-associated infection, which are considered to be the major factor of implant failure [5]. Therefore, further surface modifications are desirable to endow PEEK material with more biological properties.

Many strategies have been carried out to ensure stable integration between bone tissue and PEEK implant as it is regarded as the prerequisite for long-term clinical success of implants [6], such as blending of bioactive components into, or coating with bioactive materials onto, PEEK implants [7-9]. Nevertheless, the blended PEEK composites involve a trade-off in mechanical properties in exchange for their increased bioactivity or need expensive equipment, and the bioactive coating on PEEK substrate will break down due to the poor binding. Alternatively, the sulfonation of PEEK material to produce porous structure has been reported to be a simple and reliable way to enhance osseointegration of PEEK implant [10]. Nevertheless, it cannot balance implant's osteogenesis and antibacterial capability, lack of which may lead to secondary surgery or even amputation and death. Thus, our previously study employed the combination of silver and gentamicin to assure implant's bacteria-killing capacity [4]. However, the usage of gentamicin may elicit antibiotic resistance, which is now a serious risk to public health with more than 70% of hospital acquired bacterial infections being resistant to one or more of the antibiotics [11]. What's worse, the current slow pace of antimicrobial agent development cannot catch up with the increasing number of multidrug-resistant bacteria [12], which may put the world in the position to face an epidemic of untreatable bacterial infections. This motivates the requirement for non-antibiotic alternatives.

Copper, a well-known antimicrobial material, displayed synergistic antimicrobial activities when combined with silver [13]. Their synergistic effect has been proved to be effective against resistant bacteria, which may account for increased cell permeability [14,15]. Hence, copper was chosen to substitute for gentamicin and combine with silver. Their combination will not only qualify implant with bactericidal capacity but also endow osteogenesis and osseointegration ability to implant. The enhanced osteogenesis performance is supposed to originate from the inherent nature of copper to accelerate bone regeneration by maturation of collagen through lysyl oxidase crosslinking and by inducing osteogenic differentiation of mesenchymal stem cells (MSC) [11]. Moreover, appropriate concentration of silver, which is relatively low, also possesses osteogenesis stimulation effect [16,17]. However, whether copper and silver are bactericidal or osteogenic depends on their concentration, making the dosage level of metal ions to be critical in balancing osteogenesis and bacteria-killing.

Silk fibroin (SF), a biocompatible material, possesses different isoelectric points (pI) for different parts of its backbone, leading to the variation of electric charge and molecular conformation with the change of pH. This feature of SF could exert a pH-responsive controlled release of metal ions, consequently achieving low concentration of metal ions for osteogenesis under physiological environment and high concentration of metal ions needed for efficient bacterial killing at low pH environment. This characteristic of coating could help implant achieve a fast and large amount release of metal ions only at when and where bacteria appear, as bacteria metabolism produces organic acid and acidifies their local environment [18]. Therefore, SF was chosen to be the carrier to control the release of metal ions.

However, the two performances of osteogenesis and bacteria-killing may not be able to guarantee rapid osseointegration and long term stability of implants, as blood vessels not only transport essential oxygen and nutrients but also delivery osteogenic cells and factors to the region of bone defect [19]. Furthermore, it has been reported that accelerated angiogenesis can lead to earlier osseointegration [20]. Thereby, equipping implants with angiogenic potential would be beneficial to the integration between bone tissue and implants. Fortunately, the copper chosen before can not only strengthen osteogenesis and bacterial killing capability, but also promotes angiogenesis by artificially mimicking hypoxia through stabilizing the structure of hypoxia-inducible factor (HIF- 1α) which in turn stimulating the secretion of VEGF [21].

In this study, we therefore designed a three-dimension (3D) porous microstructure into PEEK surface first. Then dopamine was polymerized on the surface of PEEK as a bridge for the introduction of copper and silver loaded SF. This designation was aimed to achieve the rapid osseointegration of PEEK implants even in the face of the bacterial infection, which can result in successful bone defect repair. In vitro and *in vivo* experiments were carried out to verify our hypothesis.

2. Materials and methods

2.1. Preparation of Ag nanoparticles decorated porous CuO microspheres (μCuO/nAg)

The process of μ CuO/nAg production is listed in Fig. 1a. Firstly, the porous copper oxide microspheres (μ CuO) were prepared by a hydrothermal method. Specifically, 2.57 g of copper nitrate hydrate Cu(NO₃)₂•3H₂O was mixed with 80 mL of ethanol, 60 mL ammonia-water and 20 mL of sodium hydroxide (1 mM). This mixture was transferred into a hydrothermal reactor and heated at 130 °C for 4 h. After that, μ CuO were collected by centrifugation followed by washing three times with deionized (DI) water and then dried in an oven at 60 °C for 12 h.

The produced μ CuO were added into 2 mg/mL dopamine solution (10 mM Tris-HCl buffer, pH = 8.5; Aladdin) with CuSO₄ (5 mM) and H₂O₂ (19.6 mM) and kept stirring for 2 h, followed by centrifuging at 8000 rpm to collect polydopamine (PDA) coated μ CuO. Then the collected microspheres were added into silver nitrate solution (10 mM, 30 mL) and kept stirring for 6 h. After that, μ CuO/nAg could be collected through centrifugation.

2.2. Preparation of silk fibroin solution

Silk fibroin solution was prepared as previously described [22]. Briefly, silkworm cocoons were cut into pieces, boiled in an aqueous solution with $0.02~M~Na_2CO_3$ for 30 min, and then rinsed in DI water. After drying at room temperature, the silk fibroin was dissolved into LiBr solution (9.3 M) at 60 °C till the solution become transparent and amber in color. Then, this solution was dialyzed against DI water using dialysis bags (MEMBRA-CEL, 12,000–14,000 MWCO) under stirring for 48 h before centrifuging at 8000 rpm for 20 min to remove the impurities, thus yielding a 7-8% (w/v) silk fibroin solution.

2.3. Surface functionalization of PEEK

Medical grade PEEK (KetaSpire, Solvay, Belgium) material was used in this study. It was purchased in rod shape and then was machined into disc shape with dimension of Φ 15 mm \times 1.5 mm for in vitro studies while rod shape with 2 mm in diameter and 6 mm in length for animal evaluation. All the samples were mechanically polished up to 2000 grits and then ultrasonically washed in acetone and ethanol.



Fig. 1. Schematic illustration of (a) $\mu CuO/nAg$ fabrication and (b) surface functionalization of PEEK.

The surface modification strategy for PEEK is depicted in Fig. 1b. PEEK material was treated with concentrated sulfuric acid (95–98 wt. %, Aldrich Chemical Corp) for 5 min under ultrasonic agitation followed by hydrothermal treatment at 100 °C for 4 h (labeled as SP). Then samples were immersed into 2 mg/mL dopamine solution (10 mM Tris-HCl buffer, pH = 8.5) under constant vibration at 37 °C for 12 h. After that, silk fibroin solution (5% w/v) with μ CuO or μ CuO/nAg was spun onto samples three times, followed by the coating of another three silk layers. The sample incorporated with μ CuO was labeled as SP-CuO while the sample incorporated with μ CuO/nAg was labeled SP-CuO/Ag.

2.4. Surface characterization

Field-emission scanning electron microscope (FE-SEM, S-4800, Hitachi, Japan) was utilized to observe the surface morphology and microstructure of coatings. For compositional analysis, X-ray photoelectron spectroscopy (XPS, Kratos, UK) was employed. For surface hydrophilicity, SL200B contact angle system (Kino, USA) was utilized.

2.5. Cu^{2+} and Ag^{+} release into phosphate buffer solution (PBS)

To investigate the release behavior of Cu^{2+} and Ag^+ into PBS, inductively coupled plasma-atomic emission spectrometer (ICP-MS, Agilent 7700, USA) was utilized to measure the concentration of ions in the solution. Briefly, specimens (SP-CuO and SP-CuO/Ag) were immersed into 2 mL of PBS with different pH (pH = 7.4, 5.0) at 37 °C for 28 days. At predetermined time points, the entire volume of solution was collected and samples were refilled with fresh PBS. The concentration of Cu^{2+} and Ag^+ in the collected solution was determined by ICP-MS.

To further explore pH responsive release of metal ions, samples were immersed in 2 ml of PBS with pH of 7.4 in the first week and then immersed in PBS with pH of 5.0 for another seven days. The solution was collected and refilled at predetermined time points and the concentration of metal ions was determined by ICP-MS.

2.6. Bacteria culture and inoculation

Gram-negative bacteria Escherichia coli (E. coli, ATCC 25922) and gram-positive Staphylococcus aureus (S. aureus, ATCC, 25923) were used and incubated in Luria-Bertani (LB) broth at 37 °C overnight. The overnight-grown bacteria were adjusted into a concentration of 1.0×10^6 colony forming units (CFU)/mL and then cultured with

different samples for predesigned time periods. All experiments and measurements were carried out in triplicate.

2.7. Antibacterial rate

To assess the antibacterial rate of samples, the number of viable bacteria was quantified by the plate-counting method after samples incubated with 1 mL of bacterial suspension in LB medium. Specifically, samples were incubated with *E. coli* in LB medium with different pH values (7.4 and 5.0) for 6 h, while samples were cultured with *S. aureus* in medium with pH 7.4 for 24 h. Then the antibacterial rate was calculated by the following formula:

Antibacterial rate (%) =
$$\frac{A - B}{A} * 100\%$$
,

Where A is the average number of bacteria colonies on the control group (PEEK samples, CFU/mL) while B is the average number of bacteria colonies on the experimental samples.

2.8. Microbial viability assay

The viability of *E. coli* adhered to the samples was assessed by the Microbial Viability Assay Kit-WST (Dojindo, Kumamoto, Japan) to determine their anti-adhesion ability. Briefly, samples were cultured with *E. coli* in LB medium with pH 7.4 or 5.0 for 6 h, then they were taken out and washed with fresh PBS before incubating with LB medium which contains 5% of WST-8 reagent. After incubated at 37 °C for 2 h, the absorbance of the solution was read at the wavelength of 450 nm by a microplate reader (Bio-RAD, USA).

To evaluate the ability of anti-attachment against *S. aureus*, samples were incubated with *S. aureus* in medium with pH 7.4 for 24 h. Then the number of viable bacteria adhered to samples was determined by plate-counting method after samples rinsed in PBS and ultrasonically for 10 min.

2.9. SEM observation of bacteria morphology

After cultured with bacteria in LB medium with different pH (7.4 and 5.0) for 6 h for anti-adherent assay or in medium with pH 5.0 for 7 d for anti-biofilm assay, samples were rinsed in PBS for three times before fixed with 2.5% glutaraldehyde and graded ethanol. Then SEM was employed to observe the morphology of adhered bacteria.

2.10. Membrane permeability measurement

Propidium iodide is a fluorescent intercalating agent that can be used to stain cell. Since it is not membrane-permeable, it is also commonly used to monitor membrane integrity. In brief, after incubated with samples in LB medium with pH 5.0 for 6 h, bacteria were collected by centrifugation and transferred into 0.85% NaCl solution which contain 3 $\mu L/mL$ PI. These mixtures were kept in dark at room temperature for 15 min, followed by measurement of fluorescent intensity by a microplate reader (SPECTRAMAX M5, MD, China) with excitation at 488 nm and emission at 630 nm. The obtained intensities were normalized to that of PEEK group.

The concentration of leaked protein in the bacteria suspension also can be an indicator of membrane permeability. Pierce BCA Protein Assay Kit (Thermo Scientific, USA) was utilized to determine the concentration of protein in the suspension after bacteria incubated with samples in PBS with pH 5.0 for 6 h.

2.11. Intracellular production of reactive oxygen species (ROS)

DCFH-DA is the most widely used probe for detecting intracellular oxidative stress. To detect the production of ROS, it was added into bacteria suspension in the concentration of 10 mM and incubated in dark condition for 30 min after bacteria cultured with samples for 6 h. This suspension was collected and centrifuged to harvest bacteria, then the same volume of PBS was added into bacteria pellets. The fluorescent intensity of this new solution was determined by a microplate reader in fluorescent mode with excitation at 488 nm and emission at 525 nm.

2.12. Measurement of Cu and Ag uptake

After cultured with samples in LB medium at pH 5.0 for 6 h, a 100- μ L aliquot of bacteria suspension was spread on agar plates for bacteria counting while the rest of it was washed in EDTA solution (1 mM) followed by three-times washing in DI water. Then bacteria were harvested and digested in HNO₃ solution (GR, Beijing Chemical Reagent Co., Ltd., China) overnight before kept at 80 °C for 30 min. Then they were diluted with DI water and analyzed by ICP-MS to determine the concentration of metal ions. The amount of metal ions was normalized to the number of bacteria.

2.13. Cell culture

The adipose-derived mesenchymal stem cells (Ad-MSC) and human umbilical vein endothelial cells (HUVEC) were used and cultured in α -minimum essential medium (α -MEM) and endothelial cell medium (ECM), respectively. Both cells were used at the passages of 3 to 5 in this study, and Ad-MSC were seeded at the density of 20,000 cells/cm² while HUVEC were seeded at the density of 40,000 cells/cm². For osteogenic assays, a cocktail of α -MEM with osteogenic factors (dexamethasone, ascorbic acid and β -glycerophosphate) was used while the 1:1 mixture of α -MEM and ECM were used for coculture system. In addition, all PEEK samples were sterilized by UV light with half hour for each side.

2.14. Adhesion and proliferation of Ad-MSC and HUVEC

Cells were seeded on samples in a 24-plate for 12 h before fixed with 2.5% (v/v) glutaraldehyde at 4 °C overnight. After dehydrating in graded ethanol, samples were coated with gold by small ion sputtering device (KYKY, China, SBC-12). Then samples were observed under SEM to analyze cell adhesion morphology. To evaluate cell proliferation, samples incubated with Ad-MSC for

1, 3 and 5 d or incubated with HUVEC for 1 and 3 d, then the culture medium with 10% of MTT (Beyotime, China) was added and incubated at 37 $^{\circ}$ C at each time point. 4 h later, the medium was replaced by the same volume of dimethyl sulfoxide (DMSO), and the absorbance of this solution was read at 570 nm through a microplate reader.

2.15. Angiogenic and osteogenic differentiation of monocultured and cocultured cells

The angiogenic differentiation performance of HUVEC was estimated by the production of NO. The griess reagent system (Promega, USA) was utilized to quantify the release of NO after HUVEC cultured with samples for 24 h. In brief, cells were lysed, and 50 μL of lysed cell solution was incubated with the reagent till a purple/magenta color appeared. Its absorbance was measured within 30 min in a plate reader at 520 nm, and the amount of NO was calculated based on the prepared standard curve constructed with sodium nitrate.

For the osteogenic differentiation assessment of Ad-MSC, they were seeded on samples for monoculture or seeded with HUVEC on samples for coculture. After incubation for 7 d, BCIP/NBT alkaline phosphatase color development kit (Beyotime, China) and alkaline phosphatase assay kit (Beyotime, China) were used to characterize the qualitative and quantitative of alkaline phosphate (ALP) expression, respectively. After 14 d, collagen expression was qualitatively imaged after samples stained with 0.1% solution of Sirius Red (Sigma, USA) in saturated picric acid, then samples were destained by destaining solution (0.2 M NaOH/methanol 1:1) and their absorbances were measured with a microplate reader at 570 nm. The extracellular matrix (ECM) mineralization was evaluated after 21 days' incubation. Specifically, qualitative analysis was carried out by staining with Alizarin Red S (ARS, Sigma; 2%, pH = 4.3) at 4 °C, and quantitative analysis was performed by measuring the absorbance of calcium dissolving solution (10% cetylpyridinium chloride).

2.16. Gene expression analysis

The expression of osteo-related genes were analyzed by the real-time reverse-transcriptase polymerase chain reaction (RT-PCR). After incubated with samples for 7 and 14 days, Ad-MSC pellets were lysed with TRIzol reagent (TIANGEN BIOTECH, China) to collect RNA pellets and they were converted to cDNA using a RevertAid First Strand cDNA Synthesis Kit (Thermo Fisher, USA). Subsequently, the produced cDNA was amplified by an ABI 7500 RT-PCR machine (Applied Biosystems, USA), and primers (5'-3') used in this study are listed in Table S1. The relative mRNA expression level of each gene was normalized with the housekeeping gene18S rRNA and determined by the cycle threshold (Ct) value according to the $\Delta\Delta$ Ct method.

2.17. Animal model

The bone repairing ability of samples was assessed in a tibia model in adult New Zealand white rabbit. This animal surgery was authorized by Ethics Committee of Peking University Health Science Center, and the surgical procedures were performed in accordance with Experimental Animal Ethics Branch (LA2019019). Six 3-month-old New Zealand Rabbits were randomly assigned to PEEK, SP-CuO, and SP-CuO/Ag groups. After anesthesia with pentobarbital sodium (30 mg/kg, intravenous injection), three holes (2-mm in diameter, 6 mm in depth) were drilled in the left and right tibia of rabbits, then samples were placed into the defects. The wound was closed with sutures in layers. After the operation, the rabbits were housed in separate cages in

an environmentally-controlled animal-care laboratory. Rabbits were sacrificed after 6 and 12 weeks, and their tibias were collected and fixed in 10% neutral formalin buffer for 24 h at room temperature.

2.18. Micro computed tomography (micro-CT) analysis

Micro-CT (Inveon MM CT; Siemens, Germany) was applied to analysis the newly formed bone around implants, and it was performed at 80 kV. After scanning, the two-dimensional (2D) and three-dimensional (3D) models were reconstructed using Inveon Research Workplace software (Siemens, Germany), and the bone mineral density (BMD) and bone volume over total volume (BV/TV) were determined at the same time.

2.19. Histological evaluation

After fixation in 10% neutral formalin buffer, the tibias were rinsed in DI water before dehydrated in graded ethanol, then embedded in methylmethacrylate. Afterward, the embedded samples were cut along its vertical axis into sections with a thickness of 200 μm , followed by grinding into thickness of 20 μm . Two sections were made for each specimen. One section was observed using SEM, the other section was stained with methylene blue and acid fuchsine and captured by optical microscope.

2.20. Statistically analysis

At least three samples were used for each data point, and the results were presented as mean \pm standard deviations. One-way analysis of variance (ANOVA) was utilized to measure the statistically significant difference (p) among groups, and p values < 0.05 were considered to be statistically significant.

3. Results and discussion

3.1. Preparation and characterization of implant coating

To achieve rapid osseointegration of implant even in the face of bacterial infection, a well-designed coating was constructed on the surface of PEEK (Fig. 1). A three dimensional (3D) porous structure appeared on the surface of PEEK after sulfuric acid treatment and most of these pores were between 1.0 and 3.0 µm in diameter (Fig. 2a), which is beneficial to bone regeneration and implant stability [10,23]. Then pre-produced μ CuO and μ CuO/nAg were incorporated onto this porous surface under the assistance of silk fibroin, these incorporated microparticles were scattered on this surface and coated by silk fibroin. The μCuO exhibited a flower-like porous structure with a wide range of diameter from 0.5 to 4 µm, and they are composed of thin nanosheets protruding from the core (Fig. S1a). This flower like structure contains higher surface area, and it contributes to high loading capacity of silver nanoparticles (nAg). Thus, nAg were in situ grown from porous μCuO via PDA. The resulted particles showed the existence of nanoparticles on their surface (Fig. S1b, d), and these nanoparticles were analyzed by EDS and were identified to be silver nanoparticles (Fig. S1c), verified the successful upload of nAg. On the other hand, the successful deposition of PDA and silk fibroin was confirmed by XPS analysis (Fig. 2c). The appearance of C-N group on the high resolution C 1s spectra of SP-PDA samples indicates the successful deposition of polydopamine (Fig. 2c3). Meanwhile, the increased concentration of nitrogen element, from 2.79% to 6.15% (Fig. 2d), can ascribe to the higher content of nitrogen element in polydopamine, which further reveals the existence of polydopamine. On the other hand, the higher concentration of nitrogen element in CuO/Ag coating coincides with the rich nitrogen characteristic of silk fibroin, verifying the existence of silk fibroin. However, there were no peaks of silver and copper, which may ascribe to the shielding effect of silk fibroin. Collectively, this designed coating was successfully constructed on the surface of PEEK.

The incorporated µCuO/nAg were anchored on the surface of PEEK via silk fibroin, they can only exert influences to cells and bacteria through the release of metal ions. Thus, a pH-responsive release behavior was designed to this coating in order to avoid unnecessary premature elution of metal ions, which is able to relief the concern about silver toxicity and inhibit the emergence of bacterial resistance. This characteristic was tested by immersing samples into solution with different pH values for varying time period. The released copper and silver ions were measured and their release profiles were displayed in Fig. 3a, c. At physiological environment (pH 7.4), the lowest amount of metal ions leaked from CuO/Ag coating for both Cu²⁺ and Ag⁺. With the decrease of pH value, the release amount of metal ions increased, and the highest amount of metal ions were eluted from SP-CuO/Ag samples at the lowest pH value (5.0), which were 40 μ g for Cu²⁺ and 5 μg for Ag⁺. To further verify the pH-controlled release ability of this coating, samples were kept at physiological environment for 7 days first, and then immersed into solution with pH 5.0 for another 7 days. The CuO/Ag coating displayed a slow and steady release behavior for both Cu²⁺ and Ag⁺ at pH 7.4, and the release rate dramatically increased once samples were exposed to solution with pH 5.0 (Fig. 3b, d). Taking together, it is evidently that a pH-responsive release ability was successfully endowed to this coating. This can attribute to the unique properties of silk fibroin (Fig. 3e). It consists of heavy (H) and light (L)-chain. The H-chain contains hydrophobic repetitive parts, N-terminus, and C-terminus with different isoelectric points (pI), which are 3.8, 4.6 and 10.5, respectively [24]. This feature endows silk fibroin with electronegativity at physiological pH (7.4), thus attracting positively charged metal ions through electrostatic interaction. When environment pH decreases, the protonation degree of silk fibroin is enhanced, reducing the amount of negative charge. This causes imbalance between negative and positive charge, inducing the release of metal ions. On the other hand, pH-induced conformation change also can affect the release of metal ions. Silk fibroin is an extended conformation at pH 7.4 because of the repulsive interactions among its negatively charged backbones [24]. Thus silk fibroin is able to expose its negatively charged groups to positively charged metal ions. However, the decrease of pH will mitigate the repulsive interactions and facilitate the transition from random coil to β -sheet structure, which is tighter and more compact. This leads to fewer negatively charged groups getting exposed, resulting in the release of metal ions. In addition, the decrease of pH also can promote the release of metal ions because of the accelerated oxygen dependent dissolution of metal ions from particles [25]. Collectively, these factors assure the slow release of Cu²⁺ and Ag⁺ under physiological environment and the faster and larger amount release of metal ions under lower pH environment. Thus, this coating could inhibit unnecessary premature elution of metal ions so as to alleviate the toxicity of Ag⁺ and impede the emergence of bacterial resistance. Meanwhile, a fast and large amount release of metal ions can be achieved at when and where bacteria appear, as bacterial metabolism acidifies their local environment.

3.2. In Vitro Antibacterial Evaluation

As implant-associated infections are the result of bacteria adhesion to an implant and subsequent biofilm formation at the implantation site [26], the antibacterial abilities were evaluated by short-term antibacterial test and long-term anti-biofilm assessment. Fig. 4a showed the activities of bacteria adhered on sample, which were lowest in SP-CuO/Ag group at both pH 7.4

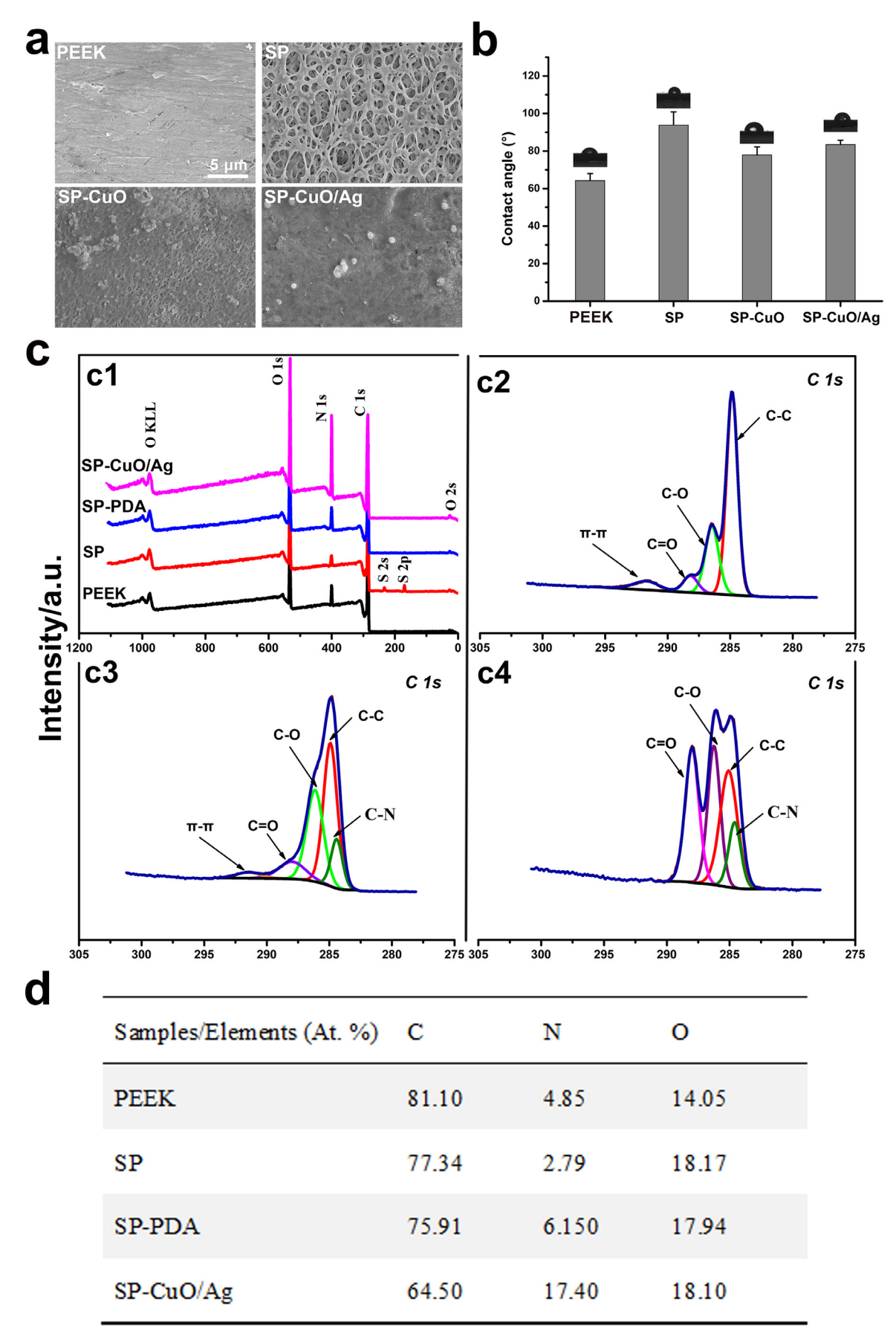


Fig. 2. (a) Surface morphology and (b) contact angle of different samples. Chemical composition of coatings: (c1) Survey spectra of XPS, and high resolution XPS spectra of (c2) C 1s from SP, (c3) C 1s from PDA, (c4) C 1s from CuO/Ag. (d) Concentration of the elemental composition on the surfaces of the functionalized coating as determined by XPS.

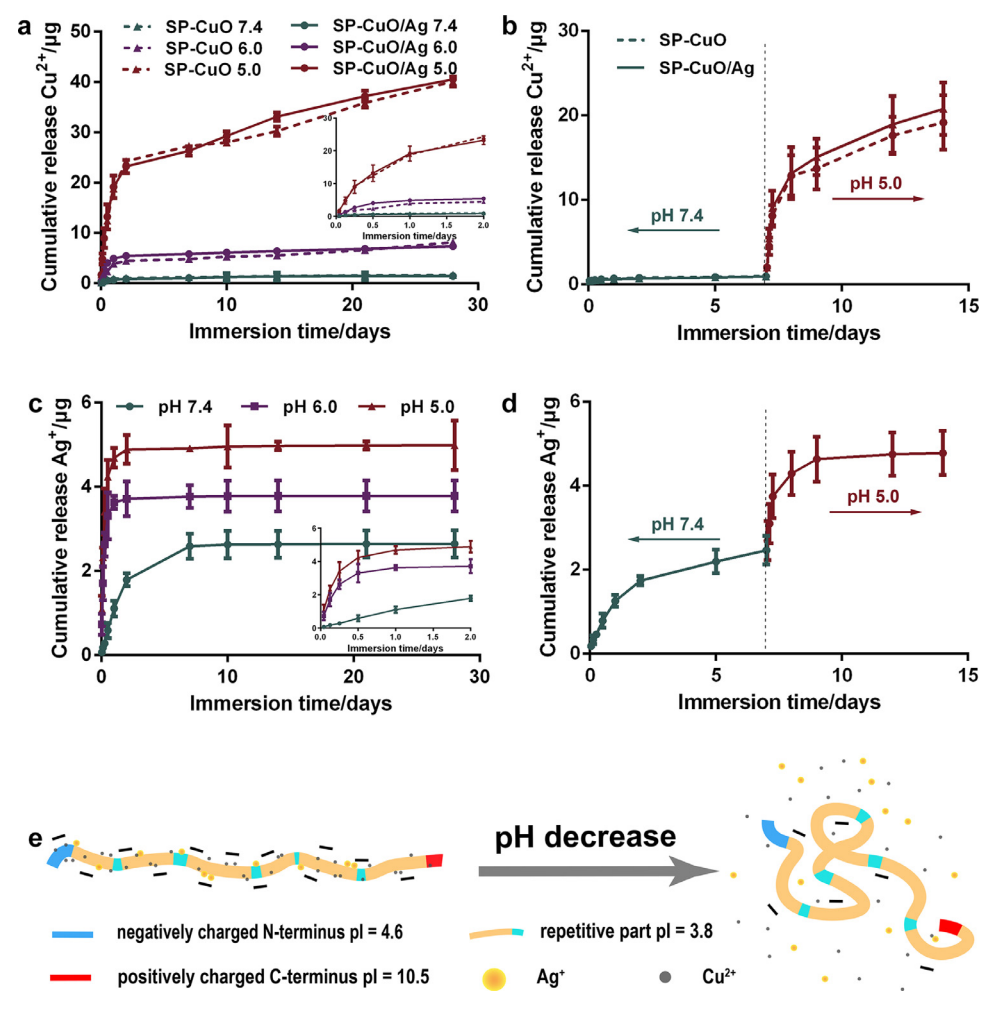


Fig. 3. The cumulative release profile of (a) copper and (c) silver at different pH condition, and pH controlled release of (b) copper from SP-CuO and SP-CuO/Ag samples and (d) silver from SP-CuO/Ag sample. (e) Silk controlled release of Cu²⁺ and Ag⁺.

and 5.0. Meanwhile, the SEM images demonstrated the same results. Fig. 4i displayed that compared with PEEK and SP-CuO samples, much fewer bacteria inhabited on the surface of SP-CuO/Ag sample when cultured at pH 7.4, and no bacteria dwelled onto SP-CuO/Ag sample when cultured at pH 5.0. These results indicated SP-CuO/Ag sample possesses the strongest anti-bacterial adhesion ability, which can hinder the formation of biofilm. However, the suspending bacteria may adhere to neighbor tissue and form biofilm, which is remarkably resistant to both the immune response and systemic antibiotic therapies [27], leading to osteomyelitis that is notoriously difficult-to-treat with treatment failure rates up to 20-30% [11]. Therefore, it appears necessary for implants to kill planktonic bacteria to block any pathways of biofilm forming. The number of viable bacteria in the suspension was lowest in SP-CuO/Ag group, whereas its antibacterial rate was the highest (Fig. 4b, c), indicating the stronger bacteria-killing ability of SP-CuO/Ag samples compare with SP-CuO and PEEK samples.

What's noteworthy, when bacterial incubated with SP-CuO/Ag samples at pH 5.0, the number of viable bacteria reached the bottom that was 1.4×10^4 CFU, 10^4 fold lower than that cultured at pH 7.4 (Fig. 4c). Consistently, the antibacterial rate under lower pH condition (pH=5.0) was higher than that under physiological environment. For SP-CuO/Ag group, the antibacterial rates at pH 5.0 and 7.4 were 99.99% and 75.62%, respectively. These results can be ascribed to the direct and indirect effects of pH variation.

The variation of pH can indirectly influence the growth of bacteria by affecting the release of metal ions, thus stimulating the pHresponsive bactericidal effect of samples. Fig. 3 displayed that the release amount of both Cu²⁺ and Ag⁺ were increased significantly with the decrease of pH value, thus leading to stronger bactericidal effect. On the other hand, the change of pH value could directly inhibit bacterial growth. As displayed in Fig. 4a, c, the number of both adherent and planktonic bacteria in PEEK group was a little bit lower at pH 5.0 than that at pH 7.4. Actually, the chosen of E. coli as experimental bacteria to evaluate the pH-responsive bactericidal effect of samples was based on the fact that E. coli is more resistant to external pH variation than S. aureus [28,29], so as to minimize the effect of pH variation on bacteria-killing performance. The results showed that the direct bacterial growth inhibition effect of pH variation was significantly smaller than the bacteria-killing ability of SP-CuO/Ag sample at pH 5.0, as pH variation in PEEK group reduced 40.74% of bacterial but led to 99.99% reduction of bacteria number in SP-CuO/Ag group. Taken together, it shows that SP-CuO/Ag sample possesses effective pH-responsive antibacterial ability. As the existence of bacteria acidifies their local environment [30], it is fair to say a CuO/Ag coating with bacteriatriggered self-defensive ability was constructed. This coating could eradicate the inhabitation of bacteria and kill 99.99% of planktonic bacteria immediately after bacteria acidify their local environment, so as to avoid the formation of biofilm. To further verify the anti-biofilm capacity, bacteria were cultured with samples for

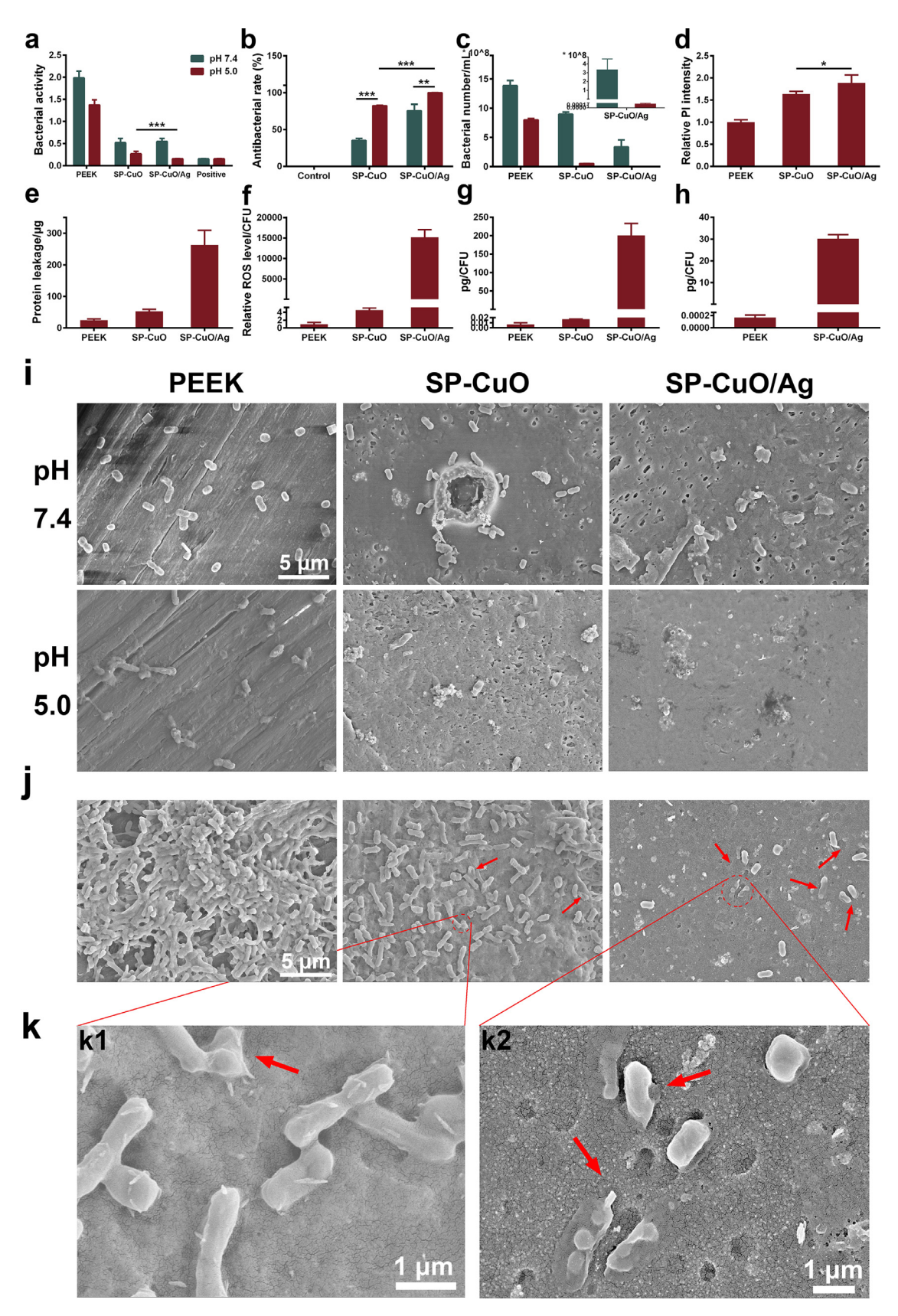


Fig. 4. *E. coli* cultured with samples in medium with different pH values for 6 h: (a) activity of bacteria adhered to different samples; (b) antibacterial rate of different samples; and (c) survived bacteria number in the culture medium of different samples. After *E. coli* treated with samples at pH 5.0 for 6 h: measurement of membrane damage through (d) relative PI intensity and (e) protein leakage; (f) quantitative analysis of relative ROS level within each bacteria; and quantitative analysis of (g) copper and (h) silver amount within each bacteria. SEM observation of bacterial morphology after cultured with samples for (i) 6 h and (j) 7 d, as well as images with higher magnification of bacteria adhered on (k1) SP-CuO sample and (k2) SP-CuO/Ag sample. Red arrows indicate bacteria with distorted shape or damaged membrane. *P < 0.05; **P < 0.01; ***P < 0.01.

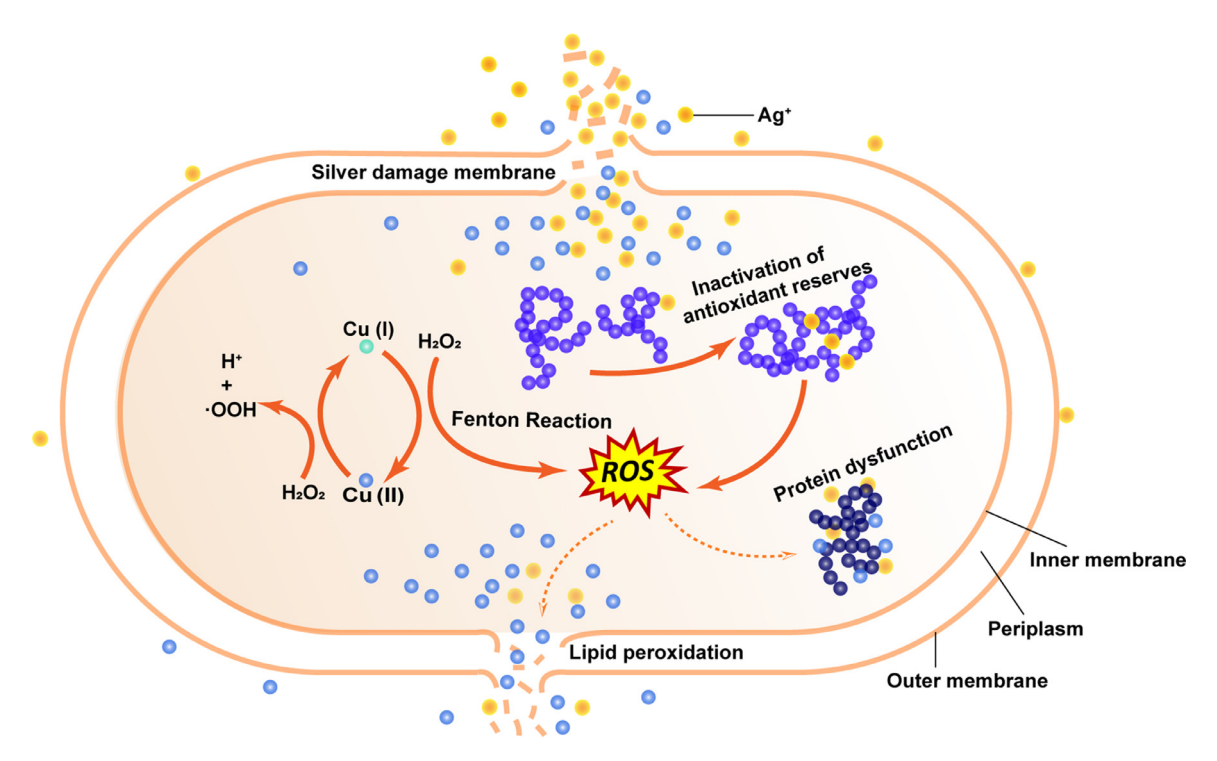


Fig. 5. Schematic illustration of synergistic bactericidal effect between copper and silver.

7 days. Fig. 4j displayed that a biofilm was formed on the surface of PEEK sample and lots of bacteria resided upon SP-CuO sample, while only a few bacteria scattered upon SP-CuO/Ag sample with distorted or even broken shape. The magnified images further demonstrated the damaged morphologies of bacteria. Fig. 4k1 presented the distorted morphology of bacteria that adhered on SP-CuO sample while Fig. 4k2 clearly exhibited the broken membrane of bacteria that adhered on SP-CuO/Ag sample. This proved the extraordinary effect of SP-CuO/Ag samples against bacterial infection, which can guarantee the victory of host cells in the "race to the surface" [31].

It's noticeable that SP-CuO/Ag sample killed 99.99% of bacteria. The difference in antibacterial ability between SP-CuO group and SP-CuO/Ag group indicated that the combination of copper and silver should be able to enhance bacteria-killing capability. Copper and silver were reported to kill bacteria through different pathways. Specifically, copper can impair bacterial membrane functions through lipid peroxidation, while silver will coordinate with particular sites of membrane leading to compromised integrity of bacterial membrane or disruption of bacterial electron transport chain activity [32-34]. Also, both of them can increase intracellular ROS but copper tends to elevate the production of ROS through catalyzing Fenton chemistry and hydroxyl radical formation, while silver mainly depletes antioxidant reserves thus resulting in increased intracellular ROS [35-37]. As to the dysfunction of protein, copper can oxidase the amino acid side chain in protein causing inactivity, while silver can displace with metal ions leading to inhibition of protein activity [38,39]. Therefore, we postulated that the combination of copper and silver would exhibit synergistic antibacterial capability, which could result in severer disruption of membrane/protein and enhanced accumulation of intracellular ROS. To verify these hypotheses, the membrane integrity was monitored through direct and indirect assays, and the intracellular ROS level was measured. As depicted in Fig. 4d, the SP-CuO/Ag group possessed higher PI intensity than SP-CuO group, directly indicates more serious damage to bacterial membrane in SP-CuO/Ag group. Meanwhile, indirect assays further confirmed this result. Fig. 4e demonstrated that much higher protein leakage appeared in SP-CuO/Ag group rather than SP-CuO group, while much higher intracellular copper and silver concentration in SP-CuO/Ag group was illustrated in Fig. 4g, h. As to the intracellular ROS level, the combination of copper and silver imposed significant effect on it, elevating the intracellular ROS level by thousands of times (Fig. 4f). These results perfectly validated our hypothesis and from which a more detailed bacteria-killing mechanism could be deduced (Fig. 5). Taken these results together, we reason that the combination of copper and silver could cause severer membrane disruption than copper alone, which can lead to a higher amount of protein leakage and a higher concentration of intracellular metal ions. Boosted intracellular accumulation of ROS and more serious protein dysfunction would happen because of the elevated concentration of intracellular metal ions. These together would finally lead to stronger antibacterial ability. In addition, the antibacterial ability of SP-CuO/Ag sample against E. coli can be applied to S. aureus - more prevalent source of implant infection. To some extent, the thick wall of S. aureus would undermine the ability of copper and silver to get inside bacteria, but that would not exert significant influence on the antibacterial ability of SP-CuO/Ag sample to E. coli and S. aureus. Because copper and silver can destroy the membrane structure of S. aureus through silver binding to thiol-group of the membrane and lipid peroxidation elicited by copper [32,40,41]. Besides that, they also can kill bacteria through other different pathways, i.e.: ROS production, protein dysfunction, enzyme inactivation, and DNA damage, all of which are applicable to different bacteria, including S. aureus. The results of SP-CuO/Ag against S. aureus further proved these statements. As depicted in Fig. S2, after cultured with S. aureus in medium at pH 7.4 for 24 h, SP-CuO/Ag sample killed 99.99% of planktonic S. aureus. Besides, SP-CuO/Ag sample significantly inhibited the adhesion of *S. aureus* as the number of S. aureus adhered on SP-CuO/Ag sample and PEEK sample were around 600 CFU/cm² and 3.7×10^7 CFU/cm², respectively.

3.3. Adhesion, proliferation, and osteodifferentiation of Ad-MSC

Cell adhesion and proliferation were assessed as it is fundamental of osseointegration [42]. SEM was used to observe the morphology of cells. After cultured for 12 h, cells adhered upon SP-CuO and SP-CuO/Ag samples displayed a polygonal shape with extended filopodia to sense the substrate while cells on PEEK surface exhibited more spreading morphology (Fig. 6a). However, the proliferation of cells showed best results on SP-CuO sample (Fig. 6b), revealing facilitated cell proliferation by the incorporated copper. Meanwhile, there was no significant difference about cell proliferation between SP-CuO and SP-CuO/Ag samples, indicating the existence of silver did not impose toxicity to cell proliferation. Apart from that, the combination of copper and silver even facilitated the osteogenesis of cells compare with CuO coating. After cultivation for 7 d, ALP activity, which plays a major role in bone mineralization and serve as a phenotypic marker for osteoblast cells, was highest in SP-CuO/Ag group (Fig. 6d), and its staining images displayed the deepest blue color and largest staining area in SP-CuO/Ag group (Fig. 6c), which means the strongest expression of ALP in SP-CuO/Ag group. Consistently, qualitative and quantitative of collagen secretion and calcium deposition highlighted the osteogenesis ability of SP-CuO/Ag sample (Fig. 6e, f, g, h). Largest staining area and deepest red color for both Sirius red and ARS staining appeared on SP-CuO/Ag sample, and the quantitative results were in accordance with the staining

To further investigate the osteodifferentiation of Ad-MSC on different samples, the expression of some osteo-specific markers need to be measured as cells tend to express various biomarkers in different stages of differentiation. Generally, there are three stages in the osteodifferentiation of MSC: proliferation, matrix maturation, and matrix mineralization [43]. Accelerated cell growth and enhanced ALP expression happened during the first stage. During the second stage, the secretion of collagen type I (COL I) matrix, which is the major component of extracellular matrix and dominate protein source of the organic part of bone [44], would be heightened. The third stage is featured by facilitated production of the extracellular protein, OCN, and subsequent deposition of calcium phosphate mineral [45]. Therefore, the expression level of genes that encoding ALP, COL I, and osteocalcin (OCN) were quantitated by RT-PCR (Fig. 6i). The expression of ALP in SP-CuO/Ag group was half of that in PEEK group at day 7, and was upregulate to be four-fold of that in PEEK group at day 14. The expression of COL I demonstrated the same pattern. Ad-MSC cultured on SP-CuO/Ag demonstrated the lowest level of COL I expression at day 7, which increased to be the highest at day 14. As to OCN, its expression level in SP-CuO/Ag group slightly fell behind that of PEEK group at day 7, whereas it caught up and became the highest at day 14.

Concluded from these results, it is evidently that the combination of copper and silver could potentiate the osteogenesis of cells compare with SP-CuO group, indicating that the incorporated silver could stimulate osteogenesis. Actually, many studies reported that silver nanoparticles did facilitate osteogeneic differentiation of stem cells at an appropriate concentration [46-48]. It was documented to account for the exposure of nAg to cells, triggering the upregulated expression of cbfa1 or mitogen-activated protein kinase (MAPK) [49,50], both of which are involved in the regulation of osteoblast differentiation. In addition, the effect of copper on the enhanced osteodifferentiation cannot be ignored. Copper has been proved to promote cell proliferation and differentiation at relative low concentration (0.1 mM/6.4 µg/mL) [51]. After incubated at physiological environment for 28 d, the release amount of Cu²⁺ from SP-CuO/Ag samples was only 0.85 μg/mL, and it could be even lower when cultured with cells because of the barrier effect of extracellular matrix secreted by cells [48]. This low concentration of Cu²⁺ will not exert adverse effect to cell activities and conversely would be beneficial to cell proliferation and osteodifferentiation. Together, these solidly support that the CuO/Ag coated PEEK sample can elevate cell proliferation and osteogenesis.

3.4. Adhesion, proliferation, and differentiation of HUVEC

It has been reported that accelerated angiogenesis can lead to earlier osseointegration through the delivery of osteogenic precursors to, and direct formation of bone on, the implant surface [20]. Therefore, the angiogenesis performances of samples were evaluated. SEM was applied to observe the adhesion of cells (Fig. 7a). It showed that a relatively spherical shape of HUVEC appeared on the surface of PEEK, and the cells adhere on SP-CuO sample became somehow elongated. Meanwhile, the counterparts on SP-CuO/Ag sample manifested flat morphology with lamellipodia stretching out to sense the substrate. These results together disclose the preference of HUVEC to SP-CuO/Ag sample. The following proliferation activity was evaluated by MTT method. The PEEK sample exhibited the highest cell activity at day 1, whereas both SP-CuO and SP-CuO/Ag groups caught up and presented superior cell activity at day 3 (Fig. 7b). The production of NO, a mediator of angiogenesis, was measured as it can drive ECs differentiate towards mature blood vessels [52]. As depicted in Fig. 7c, there was no significant difference in the production of NO between SP-CuO/Ag group and SP-CuO group, which was more than twice as much as that of the PEEK group.

Given these findings, the employment of silver did not undermine the angiogenesis potential of HUVEC, and the utilization of copper did favor the angiogenesis of HUVEC. In fact, it was reported that copper can induce angiogenesis through activating an extracellular target (perhaps pro-angiogenic cytokine) [53]. Apart from that, copper was believed to elicit angiogenesis through endocellular pathway. Specifically, copper can strengthen the hypoxia stimulus by stabilizing the structure of hypoxia inducible factor- 1α (HIF- 1α), in turn inducing the transcription of vascular endothelial growth factor (VEGF), activating endothelial nitric oxide synthase (eNOS), and increasing the release of NO [21,54], eventually leading to angiogenesis. Taken together, thanks to the controlled slow release of metal ions, the CuO/Ag coating will not attenuate the angiogenesis potential of HUVEC in spite of the existence of nAg and conversely promote the angiogenesis of HUVEC.

3.5. Osteogenesis of Ad-MSC when cocultured with HUVEC

To more closely represent the real environment of bone healing process, Ad-MSC and HUVEC were cocultured on samples and the osteogenesis performance were determined. In this coculture system, SP-CuO/Ag samples exhibited the highest capacity to promote the osteodifferentiation of cells, followed by SP-CuO and PEEK samples. What's notably, the coculture system per se, which allows the complete crosstalk between Ad-MSC and HUVEC, profoundly heightened the osteogenic activity of cells, whereas abolished their later mineralization. In detail, the staining images of ALP expression and collagen secretion in coculture system presented much larger stain area with deeper color in comparison to the monoculture of Ad-MSC (Fig. 6c, e). Consistently, after incubated for 7 days and 14 days, the quantitative results manifested a 20-fold increase of ALP activity and a 3-fold increase of collagen secretion in all groups of coculture compared with that of monoculture (Fig. 6d, f). What's surprisingly, there was no calcium deposition on samples at all after cells cocultured for 21 days (data not shown).

These results seems contradictory, but they can be well explained. The facilitated osteogenic performance in coculture system

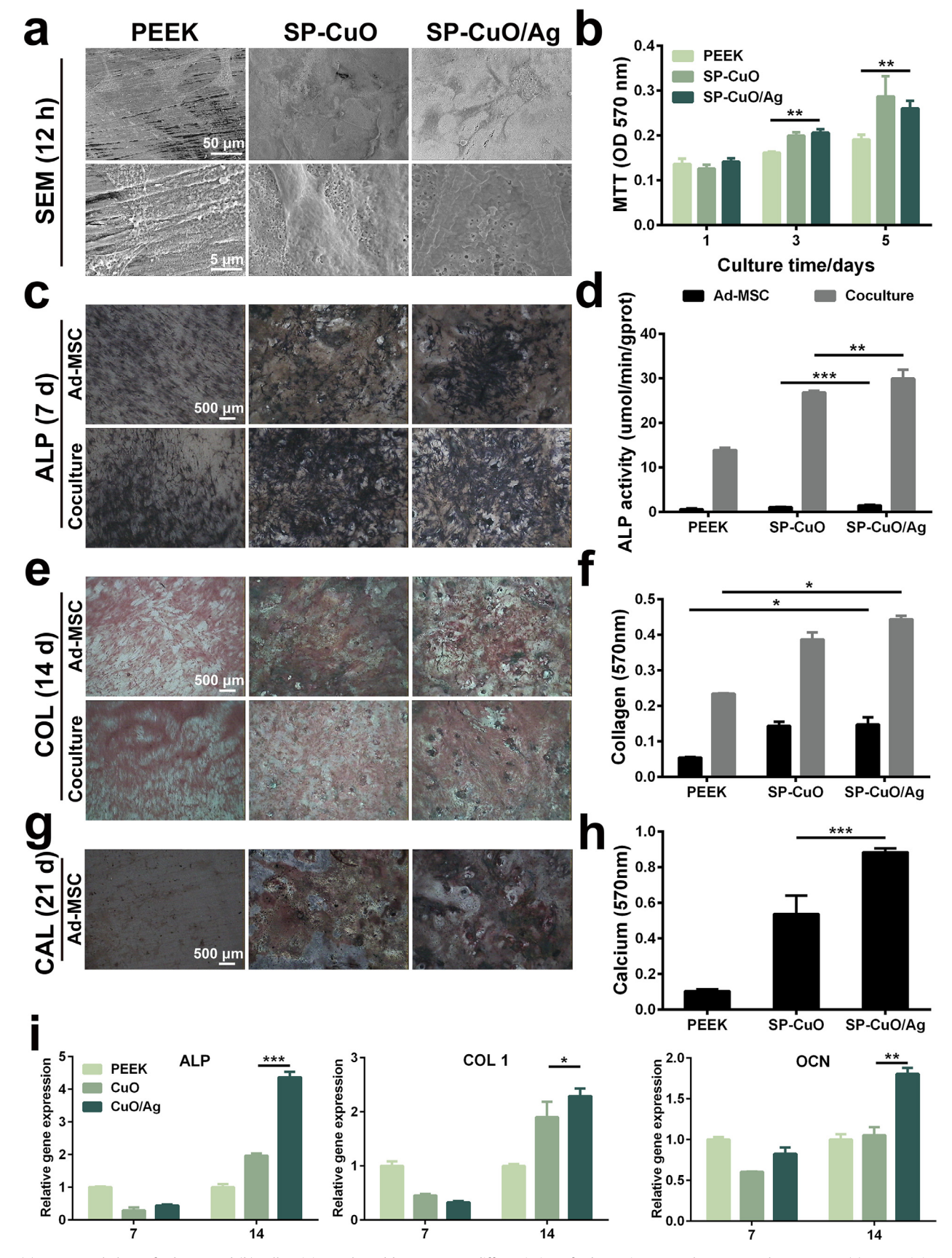


Fig. 6. (a) SEM morphology of Ad-MSC and (b) cell activity evaluated by MTT. Osteodifferentiation of Ad-MSC in monoculture or coculture system. (c) ALP staining and (d) ALP activity of Ad-MSC in different culture systems after cultured for 7 d. (e) Images of Sirius red staining and (f) quantitative analysis for collagen secretion in different culture systems after cultured for 14 d. (g) Images of Alizarin Red staining and (h) quantitative of calcium deposition after cultured for 21 d. (i) Osteogenesis related gene expression of ALP, COL 1, and OCN. *P < 0.05; **P < 0.01; ***P < 0.001; ***P

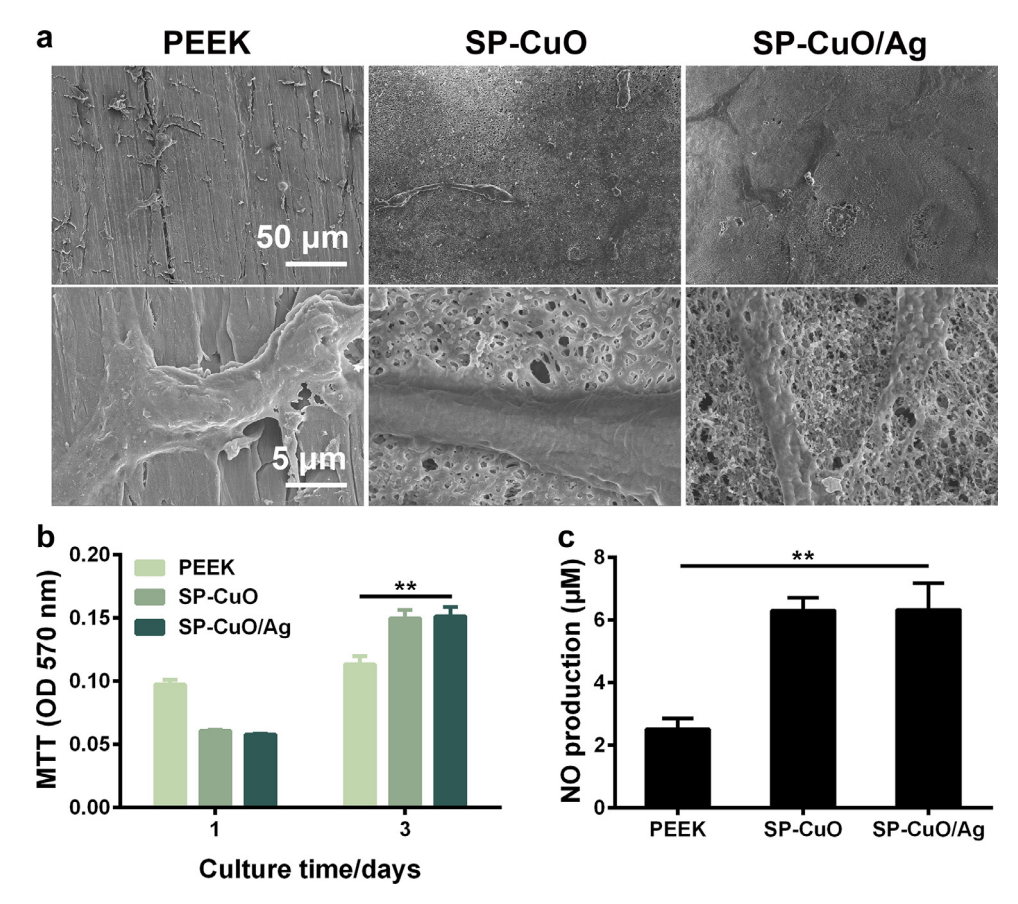


Fig. 7. (a) SEM observation of HUVEC and (b) cell activity evaluated by MTT. (c) NO production of HUVEC. *P < 0.05; **P < 0.01.

was believed to be originated from the direct cell-cell interaction and paracrine effects between Ad-MSC and HUVEC. It was reported that the expression of VEGF by MSC can somehow activate ECs and result in the significant up-regulation of BMP-2 and NO expression in ECs, which subsequently induce strengthened osteogenic differentiation of MSC [55]. Also, Ren et al believed that osteoblasts produce high level of slit homolog 3 protein (SLIT3), increasing bone formation by acting indirectly as an angiogenic factor to promote the growth of a subtype of vascular endothelium [56]. On the other hand, the inhibitory effect on calcium deposition should be imputed to the suppression of osterix (OSX) expression by HUVEC, therefore arresting MSC differentiation at a pre-osteoblastic stage, avoiding mineral deposition within vessels [57].

Taken together, it is undoubtedly that SP-CuO/Ag samples remain their ability to potentiate osteogenesis in coculture system, thus it is reasonable to expect that SP-CuO/Ag implant can stimulate the bone formation and lead to osseointegration *in vivo*.

3.6. In vivo studies

Considering the in vitro performances of CuO/Ag coated samples, which potentiated osteogenesis, angiogenesis, and antibacterial ability, it was expected to facilitate new bone formation and osseointegration *in vivo*. An established rabbit tibia model was used to examine the bone formation and osseointegration performances of implants with constructed coatings. Micro-CT was employed to evaluate the new bone formation around implants through the observation of 3D remodeling images and axial images of all groups. The formation of new bone was indicated by red arrows in axial images and it is clearly to conclude from 3D remodeling images that highest volume of new bone formed around SP-CuO/Ag implant at both 6 and 12 weeks (Fig. 8a). The

quantitative results were consistent with that, which showed that the bone volume fraction (BV/TV) was highest in SP-CuO/Ag group and compromised in SP-CuO group but still slightly higher than that of PEEK group at both 6 and 12 weeks (Fig. 8b). Additionally, compared with PEEK group, the BMD also was increased by SP-CuO implant, and it was further heightened by SP-CuO/Ag implant (Fig. 8c). Clearly, SP-CuO/Ag implant exerted more positive effect on new bone formation than PEEK and SP-CuO implants did. As to the integration between bone and implants, it was evaluated by methylene blue and acid fuchsine staining of hard tissue slices and SEM observation of hard tissue slices. According to the staining results (Fig. 9), after implantation for 6 weeks, there was a thick layer of fibrous connective tissue surrounding the PEEK implant and separating it from bone tissue, whereas the fibrous connective tissue around the SP-CuO implant was narrowed and that around the SP-CuO/Ag implant became discontinuous and much thinner. After implantation for 12 weeks, the fibrous tissue between PEEK implant and bone tissue was narrowed and replaced by new bone. Surprisingly, the fibrous tissue around SP-CuO/Ag implants was completely replaced by newly formed bone, and some new bone appeared inside some of the pore structure, indicating the osseointegration of SP-CuO/Ag implant. The SEM and elemental mapping images of hard tissue slices corroborated that results. As displayed in Fig. S3, after implantation for 6 weeks, a layer full of carbon, which is fibrous connective tissue, separated PEEK implant from bone tissue. However, this layer around SP-CuO and SP-CuO/Ag implants were narrowed. At 12-week time point, this layer around PEEK implant reduced into a small gap, and it disappeared for SP-CuO/Ag implant. Furthermore, the optical images of stained hard tissue slices can be used to evaluate the tribological characterization of surface coating, as implants will confront the mechanical stresses that come from body movements

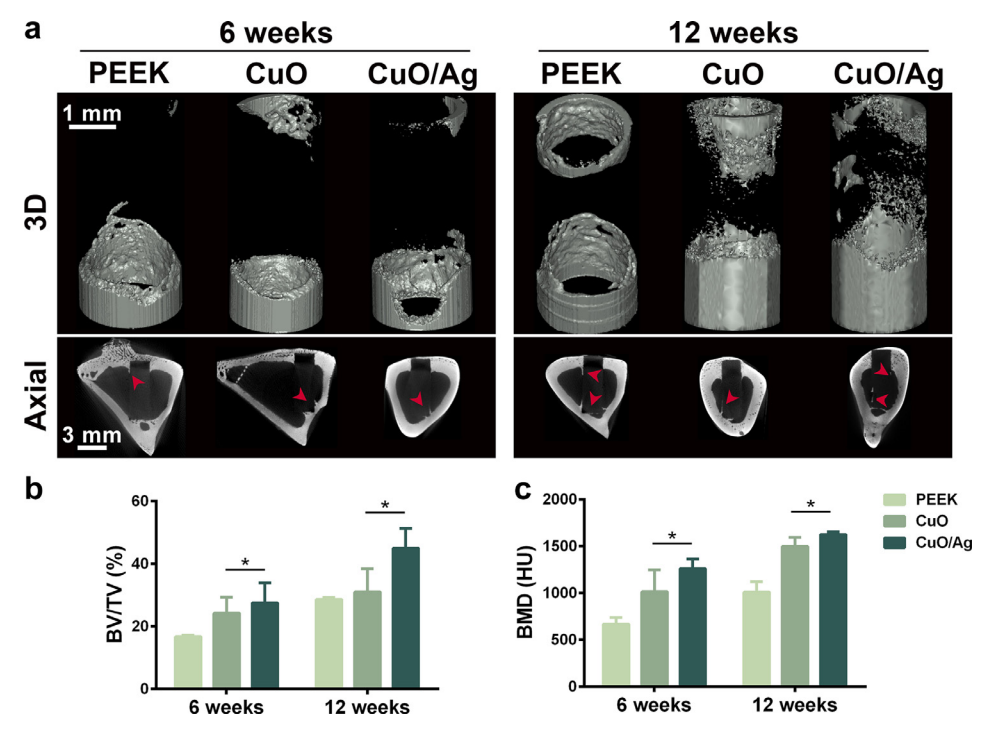


Fig. 8. Micro-CT imaging and quantification of bone regeneration. (a) 3D reconstructed micro-CT images of the new bone formation and corresponding micro-CT images of the tibia bone defect in the axial plane at 6, and 12 weeks after implantation. Quantitative histomorphometry analyses of (b) BV/TV and (c) BMD. Red arrows indicate the formed new bone around implants. *P < 0.05.

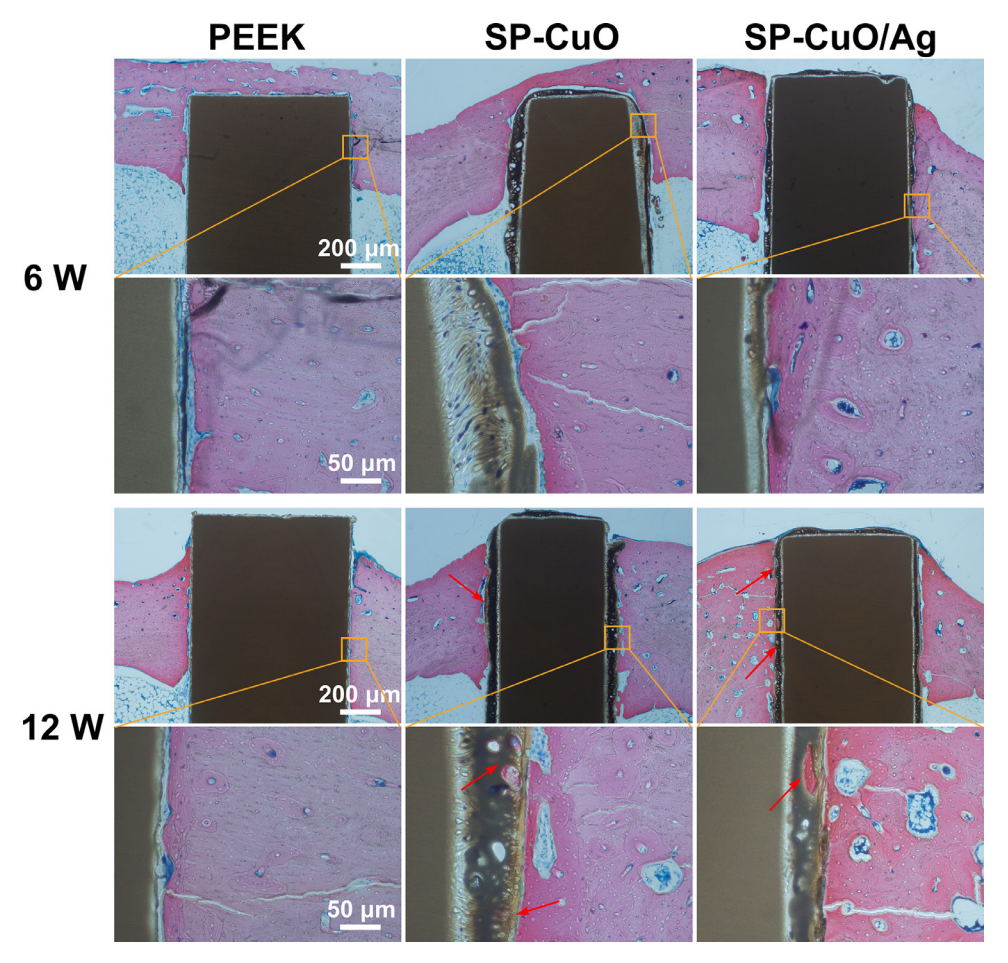


Fig. 9. After 6 and 12 weeks of surgery, the methylene blue and acid fuchsine stained hard tissue slices were observed under optical microscope and the interfaces between implants and bone tissue were magnified. Red arrows indicate new bone formed inside the porous structure of implants. (For interpretation of the references to color in this figure legend, the reader is referred to the web version of this article).

in animal study. As displayed in Fig. 9, the morphologies of surface coatings were clear, and the coatings of SP-CuO/Ag implants were relatively integrated after implanted into rabbits' tibia for 6 and 12 weeks. Moreover, there was no sign of coating peeling off from the SP-CuO/Ag implant even after implanted for 12 weeks. These results indicated coatings on SP-CuO/Ag implants are strong enough to resist mechanical stresses that come from animal movements.

Taken together, the coating constructed on SP-CuO/Ag implant is strong enough to resist mechanical stresses come from animal movements, thus it can perform its bio-functions during the entire bone healing process. Moreover, SP-CuO/Ag implant is the best choice to achieve rapid osseointegration in comparison with PEEK and SP-CuO implants. It partly stems from the incorporation of copper as which possesses inherent significant bone regeneration nature [11]. The combination of silver also can accelerate new bone formation and osseointegration through cellular behavior regulation which was elaborated previously. Moreover, Ruizhong et al stated that silver nanoparticles can stimulate fracture healing by attracting MSC, eliciting proliferation of MSC, and inducing osteogenic differentiation of MSC [50]. Hence, it is expectable for SP-CuO/Ag implant to become a successful implant that can achieve rapid osseointegration.

4. Conclusion

In this study, a pH-response coating with controlled release of copper and silver was constructed upon porous PEEK surface in order to achieve bone defect repair. The in vitro studies highlighted the osteogenic and angiogenic abilities of the silk-based CuO/Ag coatings, and its bacteria-triggered antibacterial capacity was stressed as the number of viable bacteria in medium with pH 5.0 was 10⁴ fold lower than that in medium with pH 7.4. *In vivo* studies showed higher volume of new bone around, and better bone-implant integration of, the CuO/Ag coated implant. These benefit the success of bone defect repair after the implantation of the CuO/Ag functionalized implant, leading it to be a promising coating in the future clinic application.

Data availability statement

All data generated or analyzed during this study are included in this article or supplementary information files. The raw/processed data required to reproduce these findings cannot be shared at this time as the data is also from part of an ongoing study.

Declaration of Competing Interest

The authors declare that they have no known competing financial interests or personal relationships that could have appeared to influence the work reported in this paper.

Acknowledgments

This work was financially supported by the National Key Research and Development Project (2018YFE0104200, 2018YFC1106600), National Natural Science Foundation of China (Nos. 31670974, 31370954, 51901003).

Supplementary materials

Supplementary material associated with this article can be found, in the online version, at doi:10.1016/j.actbio.2020.07.062.

References

[1] H.S. Sohn, J.K. Oh, Review of bone graft and bone substitutes with an emphasis on fracture surgeries, Biomater. Res. 23 (2019) 9.

- [2] I.V. Panayotov, V. Orti, F. Cuisinier, J. Yachouh, Polyetheretherketone (PEEK) for medical applications, J. Mater Sci. Mater Med. 27 (7) (2016) 118.
- [3] S. Balachandran, Z. Zachariah, A. Fischer, D. Mayweg, M.A. Wimmer, D. Raabe, M. Herbig, Atomic scale origin of metal ion release from hip implant taper junctions, Adv. Sci. 7 (5) (2020) 1903008.
- [4] J. Yan, W. Zhou, Z. Jia, P. Xiong, Y. Li, P. Wang, Q. Li, Y. Cheng, Y. Zheng, Endowing polyetheretherketone with synergistic bactericidal effects and improved osteogenic ability, Acta Biomater 79 (2018) 216–229.
- [5] R. Olivares-Navarrete, R.A. Gittens, J.M. Schneider, S.L. Hyzy, D.A. Haithcock, P.F. Ullrich, Z. Schwartz, B.D. Boyan, Osteoblasts exhibit a more differentiated phenotype and increased bone morphogenetic protein production on titanium alloy substrates than on poly-ether-ether-ketone, Spine J. 12 (3) (2012) 265–272
- [6] S. Parithimarkalaignan, T.V. Padmanabhan, Osseointegration: an update, J. Ind. Prosthodont. Soc. 13 (1) (2013) 2–6.
- [7] L. Hao, Y. Hu, Y. Zhang, W. Wei, X. Hou, Y. Guo, X. Hu, D. Jiang, Enhancing the mechanical performance of poly(ether ether ketone)/zinc oxide nanocomposites to provide promising biomaterials for trauma and orthopedic implants, Rsc Adv. 8 (48) (2018) 27304–27317.
- [8] H. Mahjoubi, E. Buck, P. Manimunda, R. Farivar, R. Chromik, M. Murshed, M. Cerruti, Surface phosphonation enhances hydroxyapatite coating adhesion on polyetheretherketone and its osseointegration potential, Acta Biomater 47 (2017) 149–158.
- [9] E.A. Wakelin, A. Fathi, M. Kracica, G.C. Yeo, S.G. Wise, A.S. Weiss, D.G. McCulloch, F. Dehghani, D.R. McKenzie, M.M. Bilek, Mechanical Properties of Plasma Immersion Ion Implanted PEEK for Bioactivation of Medical Devices, ACS Appl. Mater. Interf. 7 (41) (2015) 23029–23040.
- [10] Y. Zhao, H.M. Wong, W. Wang, P. Li, Z. Xu, E.Y. Chong, C.H. Yan, K.W. Yeung, P.K. Chu, Cytocompatibility, osseointegration, and bioactivity of three-dimensional porous and nanostructured network on polyetheretherketone, Biomaterials 34 (37) (2013) 9264–9277.
- [11] E.J. Ryan, A.J. Ryan, A. Gonzalez-Vazquez, A. Philippart, F.E. Ciraldo, C. Hobbs, V. Nicolosi, A.R. Boccaccini, C.J. Kearney, F.J. O'Brien, Collagen scaffolds functionalised with copper-eluting bioactive glass reduce infection and enhance osteogenesis and angiogenesis both *in vitro* and *in vivo*, Biomaterials 197 (2019) 405–416.
- [12] P.S. Stewart, J. William Costerton, Antibiotic resistance of bacteria in biofilms, Lancet 358 (9276) (2001) 135–138.
- [13] X. Chen, S. Ku, J.A. Weibel, E. Ximenes, X. Liu, M. Ladisch, S.V. Garimella, Enhanced Antimicrobial Efficacy of Bimetallic Porous CuO Microspheres Decorated with Ag Nanoparticles, ACS Appl. Mater. Interf. 9 (45) (2017) 39165–39173.
- [14] O. Torres-Urquidy, K. Bright, Efficacy of multiple metals against copper-resistant bacterial strains, J. Appl. Microbiol. 112 (4) (2012) 695–704.
- [15] J.A. Garza-Cervantes, A. Chavez-Reyes, E.C. Castillo, G. Garcia-Rivas, O. Antonio Ortega-Rivera, E. Salinas, M. Ortiz-Martinez, S.L. Gomez-Flores, J.A. Pena-Martinez, A. Pepi-Molina, M.T. Trevino-Gonzalez, X. Zarate, M. Elena Cantu-Cardenas, C. Enrique Escarcega-Gonzalez, J.R. Morones-Ramirez, Synergistic antimicrobial effects of silver/transition-metal combinatorial treatments, Sci. Rep. 7 (1) (2017) 903.
- [16] Y. Xu, B. Zheng, J. He, Z. Cui, Y. Liu, Silver nanoparticles promote osteogenic differentiation of human periodontal ligament fibroblasts by regulating the RhoA-TAZ axis, Cell Biol. Int. 43 (8) (2019) 910–920.
- [17] W. He, Y. Zheng, Q. Feng, T.A. Elkhooly, X. Liu, X. Yang, Y. Wang, Y. Xie, Silver nanoparticles stimulate osteogenesis of human mesenchymal stem cells through activation of autophagy, Nanomed. (Lond) 15 (4) (2020) 337– 353.
- [18] L. Zhao, F. Zhang, X. Ding, G. Wu, Y.Y. Lam, X. Wang, H. Fu, X. Xue, C. Lu, J. Ma, L. Yu, C. Xu, Z. Ren, Y. Xu, S. Xu, H. Shen, X. Zhu, Y. Shi, Q. Shen, W. Dong, R. Liu, Y. Ling, Y. Zeng, X. Wang, Q. Zhang, J. Wang, L. Wang, Y. Wu, B. Zeng, H. Wei, M. Zhang, Y. Peng, C. Zhang, Gut bacteria selectively promoted by dietary fibers alleviate type 2 diabetes, Science 359 (6380) (2018) 1151–1156.
- [19] B. Huang, W. Wang, Q. Li, Z. Wang, B. Yan, Z. Zhang, L. Wang, M. Huang, C. Jia, J. Lu, S. Liu, H. Chen, M. Li, D. Cai, Y. Jiang, D. Jin, X. Bai, Osteoblasts secrete Cxcl9 to regulate angiogenesis in bone, Nat. Commun. 7 (2016) 13885.
- [20] N. Khosravi, A. Maeda, R.S. DaCosta, J.E. Davies, Nanosurfaces modulate the mechanism of peri-implant endosseous healing by regulating neovascular morphogenesis, Commun. Biol. 1 (2018) 72.
- [21] E. Urso, M. Maffia, Behind the link between copper and angiogenesis: established mechanisms and an overview on the role of vascular copper transport systems, J. Vasc Res. 52 (3) (2015) 172–196.
- [22] D.N. Rockwood, R.C. Preda, T. Yucel, X. Wang, M.L. Lovett, D.L. Kaplan, Materials fabrication from Bombyx mori silk fibroin, Nat Protoc. 6 (10) (2011) 1612–1631.
- [23] L.E. Rustom, T. Boudou, S. Lou, I. Pignot-Paintrand, B.W. Nemke, Y. Lu, M.D. Markel, C. Picart, A.J. Wagoner Johnson, Micropore-induced capillarity enhances bone distribution in vivo in biphasic calcium phosphate scaffolds, Acta Biomater 44 (2016) 144–154.
- [24] A.S. Lammel, X. Hu, S.H. Park, D.L. Kaplan, T.R. Scheibel, Controlling silk fibroin particle features for drug delivery, Biomaterials 31 (16) (2010) 4583–4591.
- [25] A.M. Mittelman, A. Taghavy, Y.G. Wang, L.M. Abriola, K.D. Pennell, Influence of dissolved oxygen on silver nanoparticle mobility and dissolution in water-saturated quartz sand, J. Nanopart. Res. 15 (7) (2013).
- [26] M. Ribeiro, F.J. Monteiro, M.P. Ferraz, Infection of orthopedic implants with emphasis on bacterial adhesion process and techniques used in studying bacterial-material interactions, Biomatter 2 (4) (2012) 176–194.

- [27] E.M. Hetrick, M.H. Schoenfisch, Reducing implant-related infections: active release strategies, Chem. Soc. Rev. 35 (9) (2006) 780–789.
- [28] T. Minor, E. Marth, Growth of Staphylococcus aureus in acidified pasteurized milk, J. Milk Food Technol. 33 (11) (1970) 516–520.
- [29] J.C. Wilks, J.L. Slonczewski, pH of the cytoplasm and periplasm of Escherichia coli: rapid measurement by green fluorescent protein fluorimetry, J. Bacteriol. 189 (15) (2007) 5601–5607.
- [30] K.B. Andersen, K. von Meyenburg, Are growth rates of Escherichia coli in batch cultures limited by respiration? J. Bacteriol. 144 (1) (1980) 114–123.
- [31] C.R. Arciola, D. Campoccia, L. Montanaro, Implant infections: adhesion, biofilm formation and immune evasion, Nat Rev. Microbiol. 16 (7) (2018) 397–409
- [32] R. Hong, T.Y. Kang, C.A. Michels, N. Gadura, Membrane lipid peroxidation in copper alloy-mediated contact killing of Escherichia coli, Appl. Environ Microbiol. 78 (6) (2012) 1776–1784.
- [33] W.R. Li, X.B. Xie, Q.S. Shi, H.Y. Zeng, Y.S. Ou-Yang, Y.B. Chen, Antibacterial activity and mechanism of silver nanoparticles on Escherichia coli, Appl. Microbiol. Biotechnol. 85 (4) (2010) 1115–1122.
- [34] C.N. Lok, C.M. Ho, R. Chen, Q.Y. He, W.Y. Yu, H. Sun, P.K. Tam, J.F. Chiu, C.M. Che, Proteomic analysis of the mode of antibacterial action of silver nanoparticles, J. Proteome Res. 5 (4) (2006) 916–924.
- [35] M. Valko, H. Morris, M. Cronin, Metals, toxicity and oxidative stress, Current Med. Chem. 12 (10) (2005) 1161–1208.
- [36] L. Macomber, C. Rensing, J.A. Imlay, Intracellular copper does not catalyze the formation of oxidative DNA damage in Escherichia coli, J. Bacteriol. 189 (5) (2007) 1616–1626.
- [37] J.A. Lemire, J.J. Harrison, R.J. Turner, Antimicrobial activity of metals: mechanisms, molecular targets and applications, Nat Rev. Microbiol. 11 (6) (2013) 371–384.
- [38] M.R. Ciriolo, P. Civitareale, M.T. Carri, A. De Martino, F. Galiazzo, G. Rotilio, Purification and characterization of Ag,Zn-superoxide dismutase from Saccharomyces cerevisiae exposed to silver, J. Biol. Chem. 269 (41) (1994) 25783–25787.
- [39] L. Macomber, J.A. Imlay, The iron-sulfur clusters of dehydratases are primary intracellular targets of copper toxicity, Proc. Natl. Acad. Sci. U S A 106 (20) (2009) 8344–8349.
- [40] Q.L. Feng, J. Wu, G.Q. Chen, F.Z. Cui, T.N. Kim, J.O. Kim, A mechanistic study of the antibacterial effect of silver ions on Escherichia coli and Staphylococcus aureus, J. Biomed. Mater Res. 52 (4) (2000) 662–668.
- [41] M. Li, Z. Ma, Y. Zhu, H. Xia, M. Yao, X. Chu, X. Wang, K. Yang, M. Yang, Y. Zhang, C. Mao, Toward a Molecular Understanding of the Antibacterial Mechanism of Copper-Bearing Titanium Alloys against Staphylococcus aureus, Adv. Healthc Mater 5 (5) (2016) 557–566.
- [42] A. Chug, S. Shukla, L. Mahesh, S. Jadwani, Osseointegration—Molecular events at the bone-implant interface: A review, J. Oral. Maxillofac Surg. Med. Pathol. 25 (1) (2013) 1–4.
- [43] Z. Luo, J. Pan, Y. Sun, S. Zhang, Y. Yang, H. Liu, Y. Li, X. Xu, Y. Sui, S. Wei, Injectable 3D Porous Micro-Scaffolds with a Bio-Engine for Cell Transplantation and Tissue Regeneration, Adv. Funct. Mater. 28 (41) (2018).

- [44] H. Wu, T.W. Whitfield, J.A. Gordon, J.R. Dobson, P.W. Tai, A.J. van Wijnen, J.L. Stein, G.S. Stein, J.B. Lian, Genomic occupancy of Runx2 with global expression profiling identifies a novel dimension to control of osteoblastogenesis, Genome Biol. 15 (3) (2014) R52.
- [45] Z.F. Zhou, T.W. Sun, F. Chen, D.Q. Zuo, H.S. Wang, Y.Q. Hua, Z.D. Cai, J. Tan, Calcium phosphate-phosphorylated adenosine hybrid microspheres for anti-osteosarcoma drug delivery and osteogenic differentiation, Biomaterials 121 (2017) 1–14.
- [46] H. Cao, W. Zhang, F. Meng, J. Guo, D. Wang, S. Qian, X. Jiang, X. Liu, P.K. Chu, Osteogenesis catalyzed by titanium-supported silver nanoparticles, ACS Appl. Mater. Interf. 9 (6) (2017) 5149–5157.
- [47] H. Qin, H. Cao, Y. Zhao, G. Jin, M. Cheng, J. Wang, Y. Jiang, Z. An, X. Zhang, X. Liu, Antimicrobial and osteogenic properties of silver-ion-implanted stainless steel, ACS Appl. Mater. Interfaces 7 (20) (2015) 10785–10794.
 [48] Z. Jia, P. Xiu, M. Li, X. Xu, Y. Shi, Y. Cheng, S. Wei, Y. Zheng, T. Xi, H. Cai, Z. Liu,
- [48] Z. Jia, P. Xiu, M. Li, X. Xu, Y. Shi, Y. Cheng, S. Wei, Y. Zheng, T. Xi, H. Cai, Z. Liu, Bioinspired anchoring AgNPs onto micro-nanoporous TiO2 orthopedic coatings: Trap-killing of bacteria, surface-regulated osteoblast functions and host responses, Biomaterials 75 (2016) 203–222.
- [49] T. Verano-Braga, R. Miethling-Graff, K. Wojdyla, A. Rogowska-Wrzesinska, J.R. Brewer, H. Erdmann, F. Kjeldsen, Insights into the cellular response triggered by silver nanoparticles using quantitative proteomics, ACS Nano 8 (3) (2014) 2161–2175.
- [50] R. Zhang, P. Lee, V.C. Lui, Y. Chen, X. Liu, C.N. Lok, M. To, K.W. Yeung, K.K. Wong, Silver nanoparticles promote osteogenesis of mesenchymal stem cells and improve bone fracture healing in osteogenesis mechanism mouse model, Nanomed. (Lond) 11 (8) (2015) 1949–1959.
- [51] I. Burghardt, F. Luthen, C. Prinz, B. Kreikemeyer, C. Zietz, H.G. Neumann, J. Rychly, A dual function of copper in designing regenerative implants, Biomaterials 44 (2015) 36–44.
- [52] J.S. Isenberg, G. Martin-Manso, J.B. Maxhimer, D.D. Roberts, Regulation of nitric oxide signalling by thrombospondin 1: implications for anti-angiogenic therapies, Nat Rev. Cancer 9 (3) (2009) 182–194.
- [53] L. Finney, S. Mandava, L. Ursos, W. Zhang, D. Rodi, S. Vogt, D. Legnini, J. Maser, F. Ikpatt, O.I. Olopade, D. Glesne, X-ray fluorescence microscopy reveals large-scale relocalization and extracellular translocation of cellular copper during angiogenesis, Proc. Natl. Acad. Sci. U S A 104 (7) (2007) 2247–2252.
- [54] J.P. Cooke, D.W. Losordo, Nitric Oxide and Angiogenesis, Circulation 105 (18) (2002) 2133–2135.
- [55] H. Li, K. Xue, N. Kong, K. Liu, J. Chang, Silicate bioceramics enhanced vascularization and osteogenesis through stimulating interactions between endothelia cells and bone marrow stromal cells, Biomaterials 35 (12) (2014) 3803–3818.
- [56] R. Xu, A. Yallowitz, A. Qin, Z. Wu, D.Y. Shin, J.M. Kim, S. Debnath, G. Ji, M.P. Bostrom, X. Yang, C. Zhang, H. Dong, P. Kermani, S. Lalani, N. Li, Y. Liu, M.G. Poulos, A. Wach, Y. Zhang, K. Inoue, A. Di Lorenzo, B. Zhao, J.M. Butler, J.H. Shim, L.H. Glimcher, M.B. Greenblatt, Targeting skeletal endothelium to ameliorate bone loss, Nat. Med. 24 (6) (2018) 823–833.
- [57] T. Meury, S. Verrier, M. Alini, Human endothelial cells inhibit BMSC differentiation into mature osteoblasts in vitro by interfering with osterix expression, J. Cell Biochem. 98 (4) (2006) 992–1006.